

## AIR VELOCITY DISTRIBUTION OF THE CIRCUMFERENTIALLY ARRANGED NOZZLE GROUP

by

**Chen-Yang XU<sup>a</sup>, Li-Li WU<sup>b</sup>, and Ting CHEN<sup>b\*</sup>**

<sup>a</sup> Shandong Experimental Middle School, Jinan, China

<sup>b</sup> College of Textile and Clothing Engineering, National Engineering Laboratory for Modern Silk,  
Soochow University, Suzhou, China

Original scientific paper

<https://doi.org/10.2298/TSC1804589X>

*The air-flow field of the circumferentially arranged nozzle group is modeled and simulated. The air velocity distribution is measured using a hot wire anemometer. The results show that the simulated velocities coincide with the measured ones, confirming the effectiveness of the model. Larger rotating speeds can yield larger air velocities, indicating that introducing auxiliary air is favorable to the polymer drawing in the centrifugal spinning.*

Key words: centrifugal spinning, flow field, hot wire anemometer, simulation

### Introduction

The centrifugal spinning is a new method for fabricating nanofibers. The polymer solution or melt are extruded from the high speed rotating spinneret and attenuated into nanofibers by the centrifugal force [1-4]. Because of the years' research experience on the air drawing mechanism of melt blowing [5], our research team has been devoting to introduce the air drawing force into the centrifugal spinning. In this research, an annular air nozzle is installed around each spinneret orifice. Because the importance of the air-flow field, an experimental device made up of ten circumferentially arranged nozzles is built to form an air-flow field similar to that of the air centrifugal spinning. The air-flow field of the circumferentially arranged nozzle group is modeled and simulated numerically. The air velocities are measured with a hot wire anemometer. The simulated velocities are compared with the measured ones. The effect of the rotating speed on the air velocity is studied.

### Simulation of the air-flow field

The air-flow field model is established for the circumferentially arranged nozzle group shown in fig. 1. The most widely used  $k-\varepsilon$  model is employed as the turbulence model, which can yield accurate simulated results. The air-flow field model consists of such five equations as the continuity equation, momentum equation in the  $x$ -direction, momentum equation in the  $y$ -direction, turbulent kinetic energy equation, and turbulent dissipation rate equation.

Continuity equation:

$$\frac{\partial(\rho_a u_{ax})}{\partial x} + \frac{\partial(\rho_a u_{ay})}{\partial y} = 0 \quad (1)$$

\* Corresponding author, e-mail: tingchen@suda.edu.cn

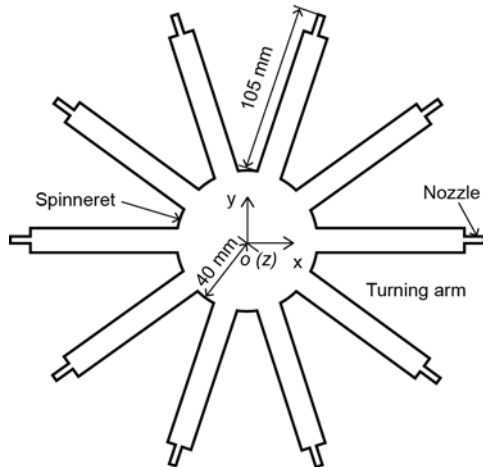


**Figure 1. Sketch of the circumferentially arranged nozzle group**

where  $\rho_a$  is the air density,  $u_{ax}$  – the  $x$ -component of the air velocity, and  $u_{ay}$  – the  $y$ -component of the air velocity.

Momentum equation in the  $x$ -direction:

$$u_{ax} \frac{\partial u_{ax}}{\partial x} + u_{ay} \frac{\partial u_{ax}}{\partial y} = F_x - \frac{1}{\rho_a} \frac{\partial p_a}{\partial x} \quad (2)$$

where  $F_x$  is the unit mass force in the  $x$ -direction, and  $p_a$  – the air pressure.

Momentum equation in the  $y$ -direction:

$$u_{ax} \frac{\partial u_{ay}}{\partial x} + u_{ay} \frac{\partial u_{ay}}{\partial y} = F_y - \frac{1}{\rho_a} \frac{\partial p_a}{\partial y} \quad (3)$$

where  $F_y$  is the unit mass force in the  $y$ -direction.

Turbulent kinetic energy equation:

$$u_a \frac{\partial(\rho_a k_a)}{\partial x} + v_a \frac{\partial(\rho_a k_a)}{\partial y} = \frac{\partial}{\partial x} \left[ \frac{v_a + \nu_t}{Pr_k} \frac{\partial(\rho_a k_a)}{\partial x} \right] + \frac{\partial}{\partial y} \left[ \frac{v_a + \nu_t}{Pr_k} \frac{\partial(\rho_a k_a)}{\partial y} \right] + (P_k - \varepsilon_a) \rho_a \quad (4)$$

where  $k_a$  is the turbulent kinetic energy of air,  $\nu_a$  – the air kinetic viscosity,  $\nu_t$  – the turbulent viscosity,  $Pr_k$  – the Prandtl number of the turbulent kinetic energy,  $\varepsilon_a$  – the dissipation rate of turbulent kinetic energy of air, and:

$$P_k = (\nu + \nu_t) \left[ 2 \left( \frac{\partial u_{ax}}{\partial x} \right)^2 + 2 \left( \frac{\partial u_{ay}}{\partial y} \right)^2 + \left( \frac{\partial u_{ax}}{\partial y} + \frac{\partial u_{ay}}{\partial x} \right)^2 \right]$$

Turbulent dissipation rate equation:

$$u_{ax} \frac{\partial(\rho_a \varepsilon_a)}{\partial y} + u_{ay} \frac{\partial(\rho_a \varepsilon_a)}{\partial y} = \frac{\partial}{\partial x} \left[ \frac{v_a + \nu_t}{Pr_\varepsilon} \frac{\partial(\rho_a \varepsilon_a)}{\partial x} \right] + \frac{\partial}{\partial y} \left[ \frac{v_a + \nu_t}{Pr_\varepsilon} \frac{\partial(\rho_a \varepsilon_a)}{\partial y} \right] + \rho_a (C_{\varepsilon 1} P_k - C_{\varepsilon 2} \varepsilon_a) \frac{\varepsilon_a}{k_a} \quad (5)$$

where  $Pr_\varepsilon$  is the Prandtl number of the turbulent dissipation rate,  $C_{\varepsilon 1}$  and  $C_{\varepsilon 2}$  are the constants in the standard  $k$ - $\varepsilon$  model.

Constants of the standard  $k$ - $\varepsilon$  model are  $C_\mu = 0.09$ ,  $C_{\varepsilon 1} = 1.44$ ,  $C_{\varepsilon 2} = 1.92$ . Turbulent Prandtl numbers are:  $Pr_t = 0.85$ ,  $Pr_k = 1.0$ ,  $Pr_\varepsilon = 1.3$ .

Another part of the air-flow field is the boundary conditions. There are three types of boundary conditions, *i. e.* the velocity inlet, the pressure outlet and the rotating wall. Air-flow field boundaries can be found in fig. 2.

- (1) *Inlet.* Each nozzle exit is considered as the velocity inlet with the initial air velocity of 60 m/s and the air temperature of 25 °C. The nozzle diameter is 0.002 m.

- (2) *Outlet.* Draw a circle with a center point of the co-ordinate origin and a radius of 400 mm. This circle will be the outlet. Because the initial air velocity is in the subsonic range, the pressure outlet can be set. The air pressure at the outlet is 101325 Pa and the air temperature is 25 °C.
- (3) *Wall.* The spinneret, turning arms and outer surface of the nozzles are set as rotating walls. They are adiabatic walls.

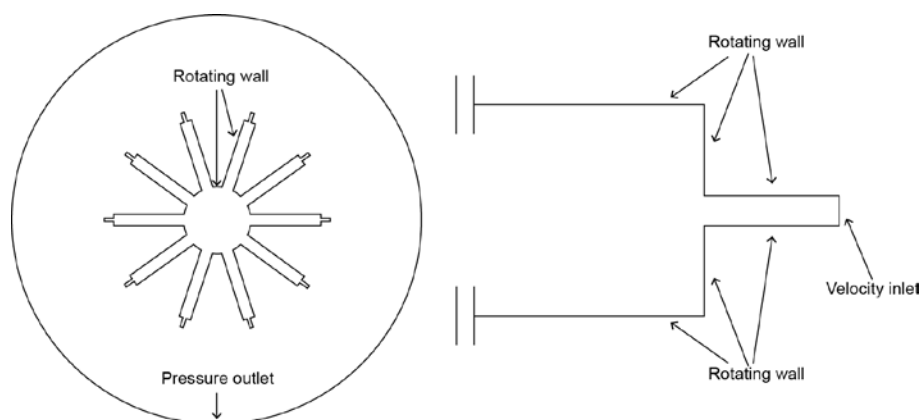


Figure 2. Boundary conditions

The CFD software FLUENT is employed to model the air-flow field. The moving reference frame (MRF) is usually utilized to deal with the counter rotation between objects in FLUENT. The basic idea of the MRF is that the air-flow field of the circumferentially arranged nozzle group is simplified as the instantaneous air-flow field by fixing the rotating spinneret at some position. The computation results show instantaneous air-flow status.

The walls in the MRF are defined as non-slip walls with a rotating speed relative to neighboring grids of 0, which means the spinneret has the same rotating speed as the fluid region. The co-ordinate origin is the origin of the rotation axis.

### Measurement of the air velocity

An IFA300 hot wire anemometer is utilized to measure the air velocities of the air-flow field. The probe is calibrated firstly. Record the electric voltages  $E_M$  and  $E_0$  of the probe at the maximum (60 m/s) and minimum (0) air velocities and obtain  $E_M$  and  $E_0$  which are 2.861 V and 1.230 V, respectively. The offset and gain are then calculated and are 1.75 and 4, respectively. Put the probe at the calibration position. Change the air velocity by adjusting the pressure regulating valve and record the corresponding electric voltage. Twelve pairs of velocity and voltage are recorded. The relational expression between the air velocity  $u_a$  and the electric voltage  $E$  is got:

$$u_a = 583.57 - 1136.59E + 788.38E^2 - 236.62E^3 + 27.11E^4$$

Air velocities at twelve positions from 0.160 m to 0.340 m away from the rotation axis are measured. The probe acquires data ten times at each position with a frequency response of 1000 Hz. The distance from the rotation axis to the nozzle exit is 0.145 m. The rotating speed of the circumferentially arranged nozzle group is changed to be 160, 560, and 960 rpm, respectively.

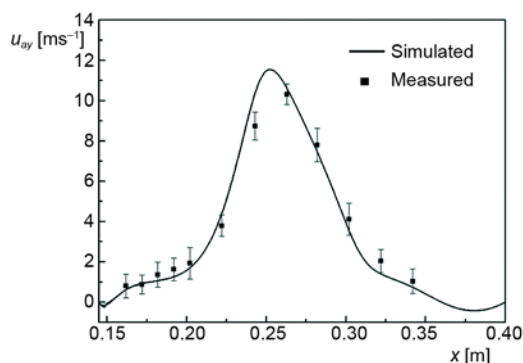


Figure 3. Air velocity at rotating speed of 160 rpm

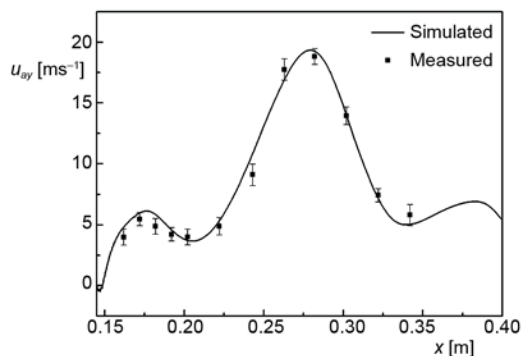


Figure 4. Air velocity at rotating speed of 560 rpm

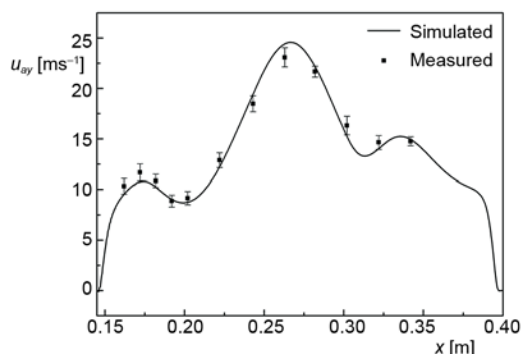


Figure 5. Air velocity at rotating speed of 960 rpm

influences of neighboring nozzles become stronger and stronger. Air velocity reaches the second also the largest peak at the position of about  $x = 0.275$  m. Shortly after that, the third peak emerges. It can be found from figs. 6-8 that the air-flow direction changes gradually from  $x$ - to  $y$ -direction with the increase of the horizontal distance, which is in accordance with the moving direction of the polymer threadline to a great extent, thus is favorable to the polymer drawing. These figures also show that larger rotating speeds can yield larger air velocities, which again makes for the polymer drawing.

## Results and discussion

Figures 3-5 show the simulated and measured air velocities at the rotating speeds of 160, 560, and 960 rpm, respectively. It can be seen that the simulated velocity curve is located within the error bars of the measured velocities in each figure, which indicates the effectiveness of the established air-flow field model. From the figures, it can be found that the air velocity increases first and then decreases as a whole. Three peaks can be seen on the air velocity profile but the middle one is the largest. With the increase of the rotating speed, the peak velocity increases and the differences between the middle peak and other two peaks decrease.

Figures 6-8 are the partial views of the air velocity vector diagram. The velocity vector diagrams explain why there are peaks on the velocity profile. Because the initial air velocity is parallel to the axis of the nozzle exit, the  $y$ -component of air velocity is 0. At the rotating speed of 160 rpm, air jets from neighboring nozzles have little interrelationships. When the air-flows a little far away from the nozzle exit, it is influenced by the neighboring nozzles and the  $y$ -component of the air velocity increases. But the  $y$ -component of the air velocity still has similar small values with that in the initial part of the air jet, which is the reason why they have similar colors on the velocity vector diagrams.

The initial air velocity is along the  $x$ -direction. When the air ejects from the nozzle, the  $y$ -component of the air velocity increases because of influences of neighboring nozzles. At the position of about  $x = 0.170$  m, the air velocity reaches the first peak as shown in fig. 5. With the increase of the horizontal distance,

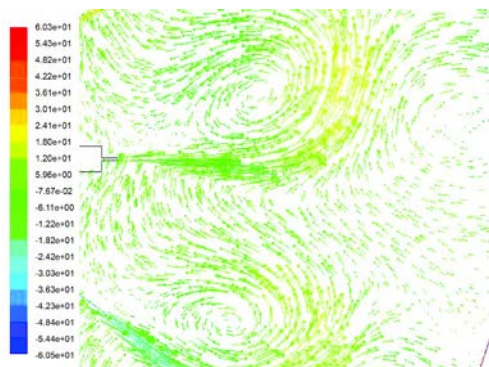


Figure 6. Air velocity vector at rotating speed of 160 rpm (for color image see journal web site)

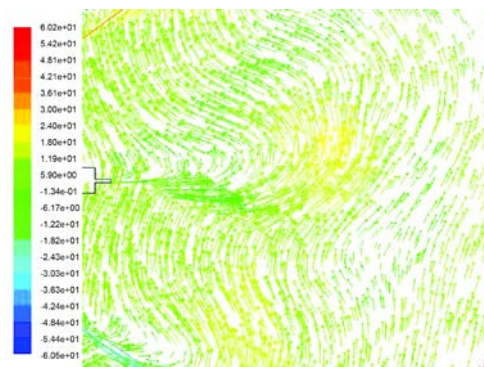


Figure 7. Air velocity vector at rotating speed of 560 rpm (for color image see journal web site)

## Conclusion

The air-flow field of the circumferentially arranged nozzle group is modeled and simulated. The air velocity distribution is measured using a hot wire anemometer. The results show that the simulated velocities coincide with the measured ones, confirming the effectiveness of the flow field model. Larger rotating speeds can yield larger air velocities. The results show that introducing auxiliary air by adding air nozzles around the spinneret is favorable to the polymer drawing in the centrifugal spinning.

## Acknowledgment

The work is supported financially by the National Natural Science Foundation of China under Grant No. 51303121, Nantong Applied Basic Research Project under Grant No. GY12016027 and Priority Academic Program Development of Jiangsu Higher Education Institute.

## References

- [1] Sarkar, K., et al., Electrospinning to Forc spinning™, *Materials Today*, 13 (2010), 11, pp. 12-14
- [2] McEachin, Z., Lozano, K., Production and Characterization of Polycaprolactone Nanofibers via Forc spinning™ Technology, *Journal of Applied Polymer Science*, 126 (2012), 2, pp. 473-479
- [3] Vazquez, B., et al., Preparation and Characterization of Polyvinylidene Fluoride Nanofibrous Membranes by Forc spinning™, *Polymer Engineering and Science*, 52 (2012), 10, pp. 2260-2265
- [4] Ren, L., et al., Large-Scale and Highly Efficient Synthesis of Micro- and Nano-Fibers with Controlled Fiber Morphology by Centrifugal Jet Spinning for Tissue Regeneration, *Nanoscale*, 5 (2013), 6, pp. 2337-2345
- [5] Wu, L. L., et al., Polymer Drawing in the Unsymmetrical Air-flow of Melt Blowing: Numerical Simulation, *Thermal Science*, 18 (2014), 5, pp. 1685-1686

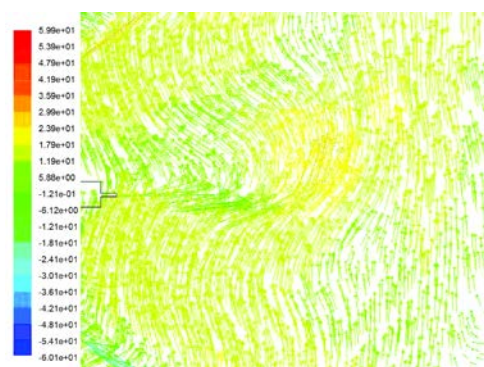


Figure 8. Air velocity vector at rotating speed of 960 rpm (for color image see journal web site)